



Dilation and energy evolution mechanisms of sandstone under true-triaxial mining unloading conditions

Wenpu Li · Ze Wang · Guorui Feng ·
Huan Zhang · Jiahui Du · Hao Li · Minke Duan

Received: 2 March 2022 / Accepted: 10 January 2024
© The Author(s) 2024

Abstract The study of sandstone dilation characteristics under actual mining and excavation conditions promotes the safe and efficient development of underground engineering. Accordingly, this study employs true-triaxial testing to reveal the influence of intermediate principal stress and unloading action in the minimum principal stress directions on rock dilation. In the stress–strain analysis, with increasing intermediate principal stress, the maximum compression of the sandstone volume in the loading and unloading tests increases, while the onset of dilation is delayed under loading conditions and initially delayed and then accelerated under unloading conditions. The energy storage limit of sandstone under the unloading test

tends to decrease with increasing intermediate principal stress, contrary to the results of the loading test, and the characteristic point at which the percentage of dissipative energy is greater than that of elastic energy occurs earlier. The energy of sandstone in the unloading test in the intermediate principal stress direction was smaller than that in the minimum principal stress direction, while the loading test showed the opposite trend. Combining these two analyses can elucidate the restraining effect and tensile stress effect of the intermediate principal stress, as well as the weakening and strengthening effects of the unloading action on the two effects. By further combining the average elastic energy and dissipative energy conversion rate

W. Li · Z. Wang · H. Zhang · J. Du · H. Li
College of Safety and Emergency Management
Engineering, Taiyuan University of Technology,
Taiyuan 030024, China

W. Li · G. Feng (✉)
Key Laboratory of Shanxi Province for Mine Rock Strata
Control and Disaster Prevention, Taiyuan 030024, China
e-mail: grfengytut@163.com

W. Li
Shanxi Province Coal-Based Resources Green
and High-Efficiency Development Engineering Center,
Taiyuan 030024, China

W. Li
State Key Laboratory Cultivation Base for Gas Geology
and Gas Control, Henan Polytechnic University,
Jiaozuo 454001, China

G. Feng
College of Mining Technology, Taiyuan University
of Technology, Taiyuan 030024, China

G. Feng
Shanxi-Zheda Institute of Advanced Materials
and Chemical Engineering, Taiyuan 030024, China

M. Duan
State Key Laboratory of Mining Response and Disaster
Prevention and Control in Deep Coal Mines, School
of Mining and Engineering, Anhui University of Science
and Technology, Huainan 232001, China

under different test conditions, the weakening effect was manifested by shortening the compressive deformation course, and the strengthening effect was manifested by developing the degree of plastic expansion deformation. This study provides important guidance for deep mining projects.

Article highlights

- Evolution law of sandstone dilation onset under different conditions
- Energy evolution on the different principal stress directions
- Average energy conversion rate of sandstone under loading and unloading conditions

Keywords Intermediate principal stress · Mining unloading · Dilation · Strain energy · Average strain energy conversion rate

1 Introduction

With the extensive utilization of underground space and mineral resources, underground engineering has gradually delved deeper (Xie et al. 2017). The mechanical properties of deep rocks differ greatly from those of shallow rocks and produce different geological hazards, which require more extensive study. One of the most frequent operations in underground engineering is mining and excavation, which often causes stress disturbances in the rock mass and disrupts the in-situ stress distribution. Since the excavation boundary is under low-constraint conditions, this disturbance produces dilatational deformation (Kaiser et al. 2000; Zhao and Cai 2010). In this case, the rock at the boundary of the excavation loses stability, and dilation occurs. The dilation of the rock occurs mainly because of the local tensile stress effect (Li et al. 2017a, b). The tensile strength of the rock is much smaller than the compressive strength; therefore, when this tensile stress effect is produced in the rock, the bearing capacity of the rock is significantly reduced. At this point, it is very easy to cause slip, rock burst, collapse, and other hazards (Wen et al. 2016), which seriously threaten the safe construction and development of underground engineering.

Therefore, the study of the dilation characteristics of the rock at the excavation boundary is beneficial for revealing the hazard mechanism in an actual excavation project, providing a theoretical basis for different mining methods and promoting the safe, economic, and efficient development of underground engineering.

In the past decades, many scholars have made great achievements by conducting conventional triaxial tests ($\sigma_1 > \sigma_2 = \sigma_3$) combined with theoretical analyses and numerical simulations to develop rock dilation properties (Zhao and Cai 2010; Kie et al. 1989; Aljano and Alonso 2005; Walton et al. 2015). However, in practical engineering, the rock mass is obviously in a complex three-dimensional unequal-stress state ($\sigma_1 > \sigma_2 > \sigma_3$) (Mogi 1967; Lu et al. 2020a), and the influence of the intermediate principal stress on the mechanical properties must be considered. The effect of intermediate principal stresses on strength was the first topic of interest. Handin et al. (1967) conducted conventional triaxial tests ($\sigma_2 = \sigma_3$) and triaxial extension tests ($\sigma_2 = \sigma_1$) and found that the compressive strength of the rock increased by approximately 15% when the intermediate principal stress was increased from $\sigma_3 - \sigma_1$. Subsequently, many researchers designed true-triaxial test apparatuses (Mogi 1967; Li et al. 2016; Feng et al. 2021b, a) and carried out a series of strength property studies (Mogi 1967, 1971; Lu et al. 2020b; Zheng and Feng 2020; Song et al. 2018; Wang et al. 2023a, b). Equally, intermediate principal stresses affect rock deformation. Within a certain range, as the intermediate principal stress increases, an increase in the principal fracture dip is observed, reflecting the shear dilatancy properties of the rock (Haimson and Chang 2000; Ma and Haimson 2016). This can also be explained by the results obtained by Zhai et al. (2020), who determined that brittle rock fractures are oriented toward a shear mechanism. It is not difficult to find that the rock will reflect certain deformation characteristics through its damage characteristics, that is, the increase in intermediate principal stress will enhance the shear deformation of the rock. However, the occurrence of rock damage is a dynamic evolutionary process, and it is difficult to analyze the entire course of rock deformation from the final damage characteristics. Therefore, it is necessary to not only focus on the effect of intermediate principal stress on the deformation characteristics of the rock after the peak but also to analyze the effect

on the dilatancy trend or dilatancy deformation before the peak. This is one of the main objectives of the current study, that is, to analyze the effect of intermediate principal stress on the dilation before the peak of the stress–strain curve.

However, the boundary dilatancy deformation caused by excavation disturbances is an important aspect in the study of rock deformation characteristics. Excavation reflects unloading action during the rock-mining process. Therefore, the unloading path should be used to determine the mechanical parameters during the practical excavation of rocks (Lau and Chandler 2004). The unloading action reduces the rock strength (Si and Gong 2020) and produces different unloading damage characteristics from those formed under the loading stress path. For example, Liu et al. (2023) use acoustic emission equipment to analyze precursor information on rock damage under loading and unloading tests. This characteristic is manifested in the evolution of microscopic cracks into macroscopic tensile cracks in rocks (Feng et al. 2021b, a). Alexeev et al. (2008) found that the brittleness of sandstone increases when it undergoes dilatancy deformation by true-triaxial tests. Apparently, this evolutionary process and brittleness enhancement are properties exhibited by dilation. Coupled with unloading in the direction of the minimum principal stress, the brittleness and tension characteristics are more prominent. Although different types of brittle rocks exhibit different damage characteristics, such as fracture tension, laminar tension, and shear tension damage, all reflect the strong damage of brittle rocks under unloading (Si and Gong 2020; Jiang et al. 2021; Wu et al. 2020; Wang et al. 2023a, b). Therefore, the generation of dilation is closely related to the unloading of boundary rocks. The pattern of fracture development in this direction as the intermediate principal stress increases is unclear and requires further research.

In summary, the intermediate principal stress and unloading action are two important factors affecting rock expansion. However, the internal mechanism of rock deformation cannot be determined only by analyzing the deformation characteristics of the rock before and at the peak of the stress–strain curve. As a result, the concept of rock energy evolution analysis has been introduced (Xie et al. 2011; Zhang et al. 2019a, b; Chen et al. 2019). The accumulation and dissipation of rock energy are closely linked to rock deformation, reflecting

the accumulation of elastic and plastic strains in rocks. Energy can also reflect the course of the crack development. For example, Ai et al. (2016) suggested that crack extension is related to the fracture energy, that is, the energy released after the peak, and the energy dissipated before the peak. Duan et al. (2020) studied rock damage by dissipating energy to further elucidate crack evolution. Thus, this paper combines stress–strain and crack evolution to analyze the effect of intermediate principal stress and unloading action on dilation.

To reveal the mechanism of sandstone expansion under true-triaxial unloading test conditions, the combined effect of intermediate principal stress and unloading action on expansion was investigated in this study. True-triaxial sandstone loading and unloading tests with different intermediate principal stresses (30, 40, 50, 60, and 70 MPa) were carried out using a multifunctional true-triaxial fluid–solid coupling test system. The strengths of sandstone under loading and unloading conditions were first fitted using the Drucker–Prager and double-shear-stress strength criteria, and then the fitting effects were compared. Subsequently, the stress–strain curves, volumetric strain–maximum principal strain relationship curves, and related energy evolution curves under loading and unloading tests were further analyzed. The energy evolution analysis encompasses different stages, different intermediate principal stresses, and different directions; a comparative energy evolution analysis is also carried out for loading and unloading tests, and the average elastic energy conversion rate and average dissipative energy conversion rate are required for evolution rate analysis. This comprehensive analysis is summarized to reveal the restraining effect and tensile stress effect of the intermediate principal stress on the sandstone. On a deeper level, the effect of unloading on the two effects of the intermediate principal stresses was explored. Accordingly, a clear understanding of the sandstone dilation mechanism under true-triaxial unloading conditions can be obtained, which provides an experimental basis for excavation engineering stability and reliability applications.

2 Experimental method

2.1 Experimental apparatus

The multifunctional true-triaxial fluid–solid coupling test system (Li et al. 2016), which was developed

independently by Chongqing University, was used in this experiment, as shown in Fig. 1. The system consists of a framed frame; true-triaxial pressure chamber; loading system; internal seal percolation system; control, data measurement, and acquisition system; and an acoustic emission monitoring system with an excellent degree of system reliability. In the loading system, a pair of independent loading devices is set in all three directions, which realizes various control methods such as force, displacement, and force–displacement, and allows for rock mechanics

and permeability tests under a variety of complex stress paths. In this test, the maximum principal stress σ_1 was applied in the Y -direction, the intermediate principal stress σ_2 in the X -direction, and the minimum principal stress σ_3 in the Z -direction.

2.2 Experimental scheme

In order to ensure the homogeneity of the internal structure and properties of the specimens, and to avoid large differences in the test results between the

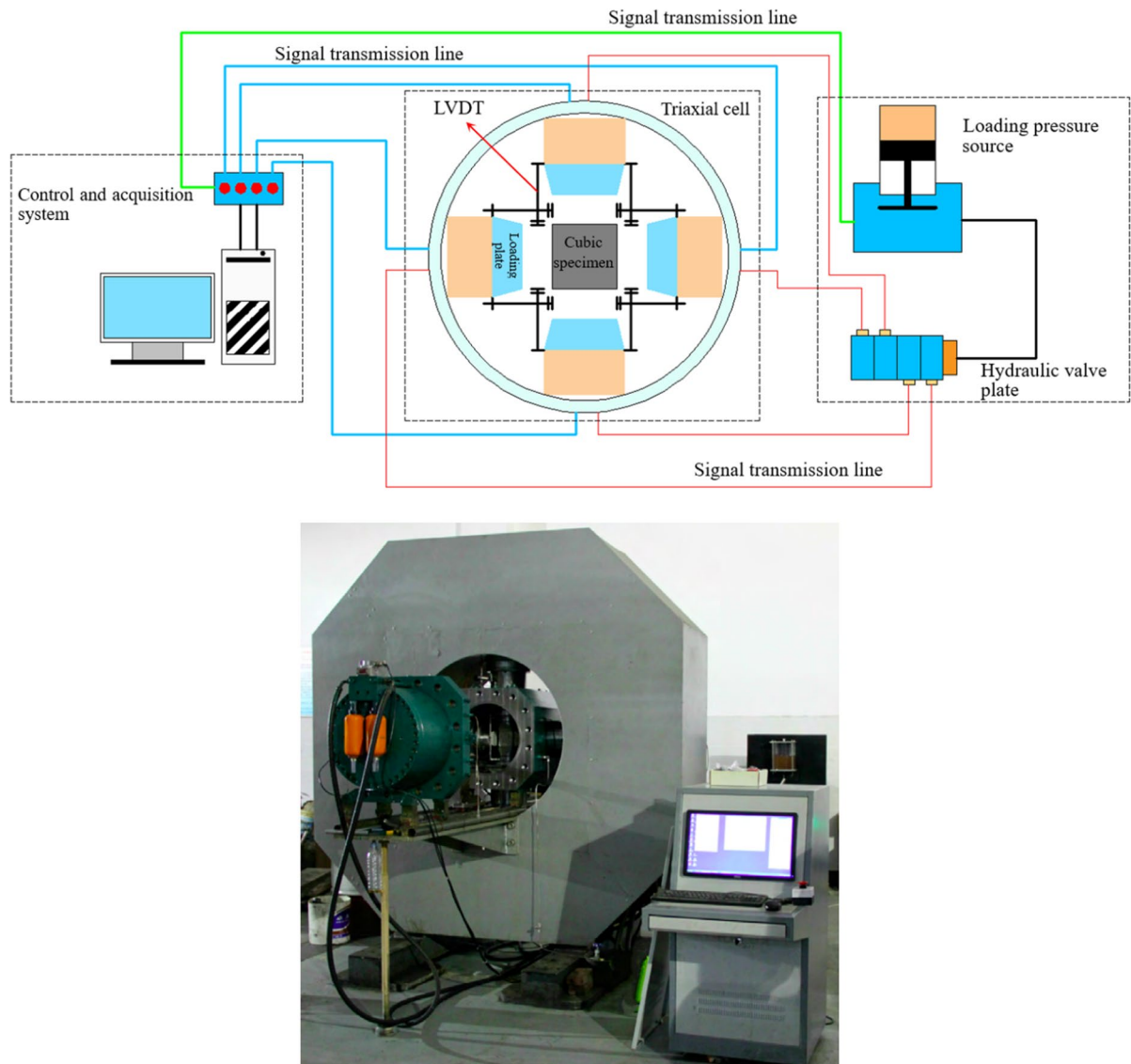


Fig. 1 True-triaxial fluid–solid coupling experiment system (Li et al. 2016)

specimens due to the dispersion, the sandstone rock samples required for the test were taken from the same piece of intact and homogeneous sandstone in the Beibei region of Chongqing, with a density of 2261 kg/m³ and a uniaxial compressive strength of 48.60 MPa. The sandstone was cut and polished into cubic specimens with 100 mm side-lengths and no obvious defects, and the end-face non-parallelism and non-perpendicularity were less than 0.02 mm. To study the mechanical properties and dilation behavior of sandstone under true-triaxial loading and unloading paths, loading and unloading tests with intermediate principal stresses of 30, 40, 50, 60, and 70 MPa were conducted.

The detailed loading path is as follows (Fig. 2a):

- (1) Loading in a force-controlled manner ($v_1 = 1$ kN/s) in the triaxial direction up to σ_{3i}
- (2) Maintaining one horizontal axial load at σ_{3i} and continuing to load the other two axial loads in a force-controlled manner ($v_1 = 1$ kN/s) up to σ_{2i}
- (3) Maintaining another horizontal axial load at σ_{2i} and loading the third axial load in a force-controlled manner ($v_1 = 1$ kN/s) up to σ_{1i}
- (4) The horizontal axial load was kept constant, and the third axial load was loaded in a force-controlled manner ($v_1 = 1.28$ kN/s) until the sandstone specimen was damaged.

The detailed unloading path is as follows (Fig. 2b):

- (1) Loading in a force-controlled manner ($v_1 = 1$ kN/s) in the triaxial direction up to σ_{3i}

- (2) Maintaining one horizontal axial load at σ_{3i} and continuing to load the other two axial loads in a force-controlled manner ($v_1 = 1$ kN/s) up to σ_{2i}
- (3) Maintaining another horizontal axial load at σ_{2i} and loading a third axial load in a force-controlled manner ($v_1 = 1$ kN/s) up to σ_{1i}
- (4) The maximum principal-stress-direction load was loaded in a force-controlled manner ($v_1 = 1.28$ kN/s) while unloading the minimum principal-stress-direction load in a force-controlled manner ($v_3 = 0.16$ kN/s) on one side until the sandstone specimen was damaged.

3 Experimental results and analysis

3.1 Analysis of sandstone deformation characteristics

Using the strain corresponding to the attainment of σ_{1i} as the starting point for strain measurement, the stress–strain relationships for different intermediate principal stress tests under loading conditions are shown in Fig. 3. The specimen underwent plastic deformation before yielding and brittle deformation after peaking (Alexeev et al. 2008). For different magnitudes of σ_2 , compressive deformation occurs in the σ_1 direction, which is the main reason for the steady increase in volume strain at the beginning of loading, while larger dilatancy deformation occurs in the σ_3 direction, which is the main factor causing sandstone dilation. The final change in the intermediate principal strain shows a decreasing trend with the

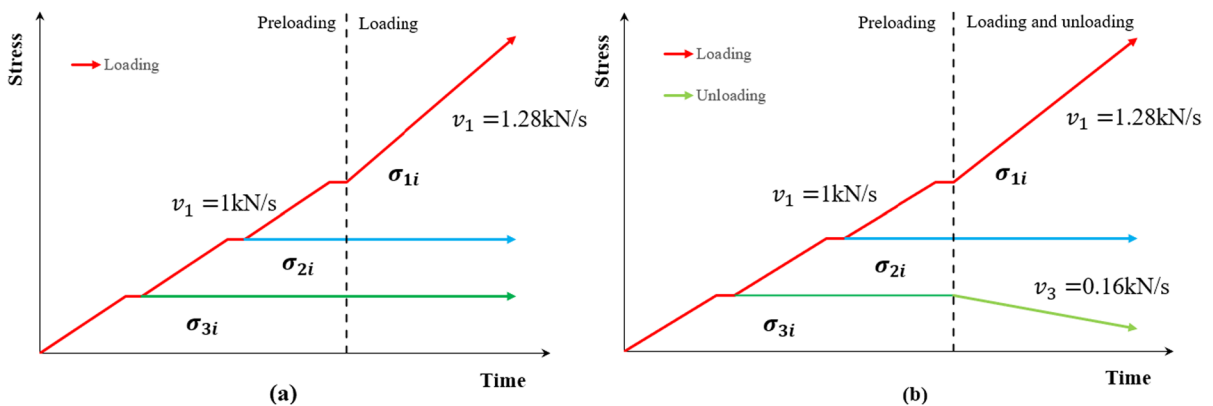


Fig. 2 Two different true-triaxial stress paths in sandstone: **a** stress path for loading test and **b** stress path for unloading test

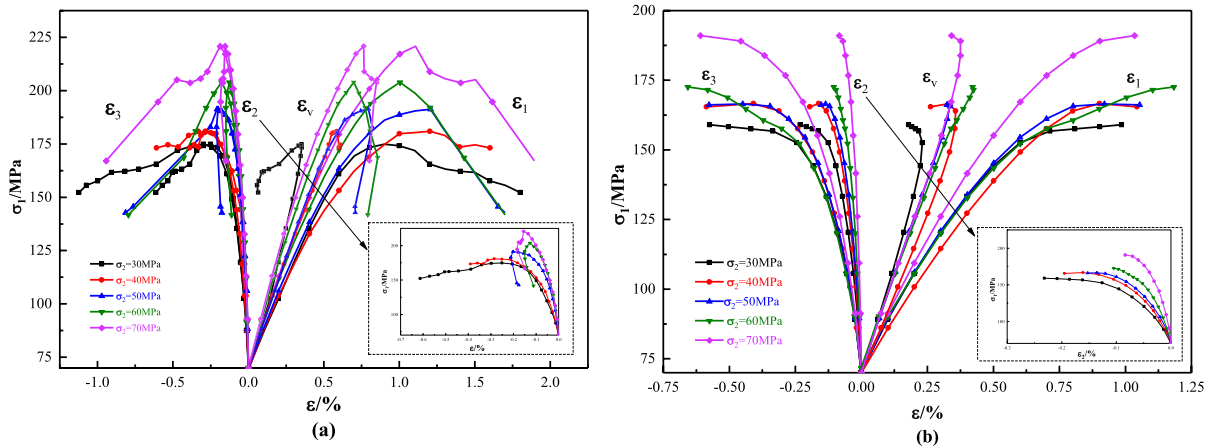


Fig. 3 Stress–strain relationships for true-triaxial tests on sandstone under different intermediate principal stress conditions: **a** loading paths and **b** unloading paths

increase in σ_2 : σ_2 increases from 30 to 70 MPa, and the maximum changes in ε_2 are 0.61%, 0.43%, 0.16%, 0.09%, and 0.13%, reflecting the restraining effect of intermediate principal stress. This restraining effect, which compresses the macroscopic cracks formed inside the sandstone specimen after σ_1 reaches the peak stress, causes the rebound deformation of ε_2 . Furthermore, this phenomenon becomes increasingly obvious with an increase in σ_2 . In contrast, ε_3 does not undergo the phenomenon of increasing rebound. This is because σ_3 is always 30 MPa, which has a small restraining effect, and the compression of the macroscopic crack produced after the peak is much smaller than the expansion in this direction, so it always remains reduced.

In particular, when σ_2 is 30 MPa, ε_v undergoes a slow phenomenon, and significant dilation occurs. In contrast, this phenomenon does not occur when σ_2 is greater than 30 MPa. This might be because the restraining effect of the intermediate principal stress is not strong when $\sigma_2 = 30$ MPa. When σ_1 is large, a horizontal tensile stress effect will occur (Gao and Tao 1993); this effect is stronger than the restraining effect, and thus a stronger dilation phenomenon occurs. When σ_2 is larger than 30 MPa, the restraining effect is larger than the tensile stress effect, resulting in almost no dilation of the specimen.

Owing to the stress control used throughout the true-triaxial damage test, only the pre-peak stress–strain relationship can be obtained under unloading conditions, as shown in Fig. 3. As can be

seen from the figure, the variation in ε_3 of the sandstone specimens is greater than the variation of ε_2 under different σ_2 magnitudes, there is a tendency for the rebound increase of ε_2 , and the slow phenomenon of ε_v occurs in all the sandstone specimens. With increasing σ_2 magnitude, the variation degree of ε_v of the sandstone specimens decreases, and the starting point of the ε_v slow increases with a delayed trend.

The effect law of unloading on the deformation characteristics of the rock can be obtained by comparing the stress–strain relationship of sandstone under loading and unloading conditions. The specifications are shown in Fig. 4. The three principal-strain growth rates and volume strain compressions under the loading test condition were larger than those under the unloading test condition, indicating that unloading weakened the elastic deformation of the sandstone, promoted the development of internal cracks, and finally reduced the strength of the sandstone. Compared with the loading test, the ε_2 value required to reach the σ_1 peak stress in the unloading test decreased and ε_3 increased. This is because the magnitude of σ_3 continues to decrease with unloading, whereas σ_3 always remains constant during the loading test. Furthermore, under the Poisson effect, the deformation in the σ_2 direction is restrained, and the deformation in the σ_3 direction is enhanced. In addition, in the loading test, the ε_v slow phenomenon occurs only when σ_2 is equal to 30 MPa, while the phenomenon occurs for different magnitudes of σ_2 in the unloading test, suggesting that the sandstone

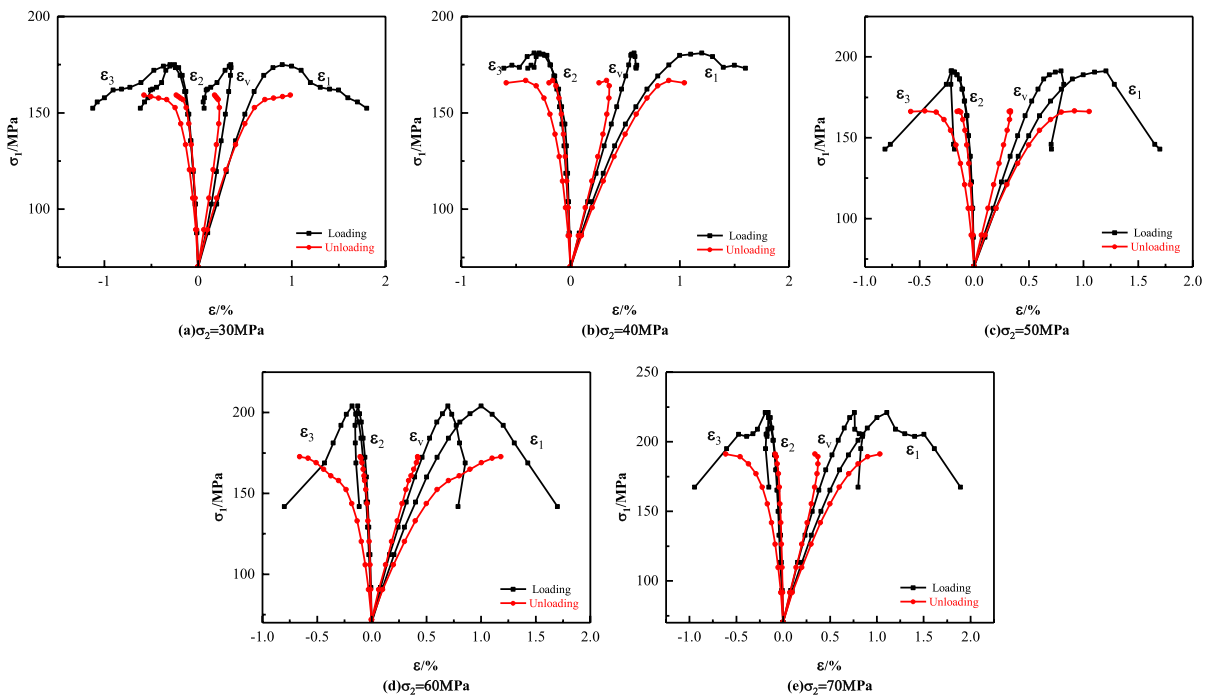


Fig. 4 Comparative analysis curves of stress–strain relationship between true-triaxial loading and unloading in sandstone under different intermediate principal stress conditions. **a–e** $\sigma_2 = 30, 40, 50, 60,$ and 70 MPa, respectively

develops cracks more fully in the σ_3 direction under the unloading test, and the rock undergoes significant dilation during the unloading process.

3.2 Analysis of sandstone strength characteristics

The unloading action not only affects the deformation of sandstone but also its strength. The peak-strength variation law of the sandstone loading and unloading maximum principal stress under different intermediate principal stresses is shown in Fig. 5. As can be seen, in the range of certain intermediate principal stresses, the peak strength of σ_1 increases for both loading and unloading conditions of sandstone as σ_2 increases, and the peak strength is greater for loading conditions than for unloading conditions at the same σ_2 magnitude. When the magnitude of σ_2 is between that of σ_3 and σ_1 , there are two effects of σ_2 : first, σ_2 counteracts a part of the local tensile stress generated by σ_1 in the direction of σ_2 , limiting the crack expansion perpendicular to the direction of σ_2 ; and second, σ_2 generates a local tensile stress along the direction of σ_3 (Gao and Tao 1993). In this study, the former and the latter are manifested

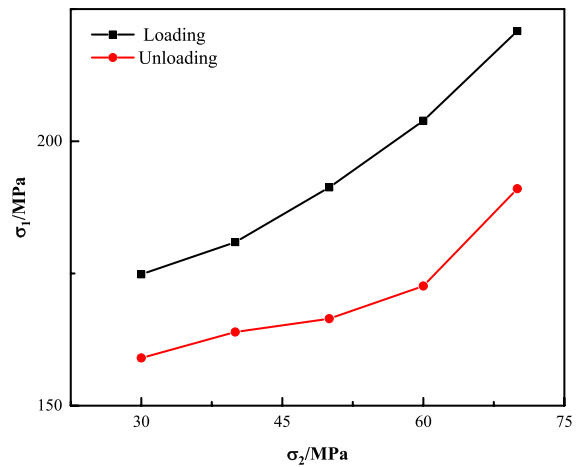


Fig. 5 Trend in peak strength for different intermediate principal stresses under loading and unloading conditions

as the restraining effect and tensile stress effect in the σ_3 direction of intermediate principal stress, respectively. Therefore, in the loading and unloading tests, σ_2 improves the strength of the rock.

To better analyze the effect of intermediate principal stress on the strength of sandstone, the Drucker–Prager strength criterion (Drucker and Prager 1952) and the double-shear-stress strength criterion (Gao and Tao 1993) were introduced for sandstone strength regression analysis, as shown in Eq. (1) and (2), respectively:

$$A_0 I_1 + \sqrt{J_2} = A_1 \quad (1)$$

$$\tau_{13} = A_0 + A_1 \sigma_m + A_2 \tau_{23} \quad (2)$$

where I_1 is the first invariant of the stress tensor; J_2 is the second invariant of the partial stress tensor; τ_{13} , τ_{23} is the principal shear; σ_m is the average stress; and A_0 , A_1 , and A_2 are the fitting parameters. The specific computational expressions are as follows:

$$I_1 = \sigma_1 + \sigma_2 + \sigma_3 \quad (3)$$

$$J_2 = \frac{1}{6} \left[(\sigma_1 - \sigma_2)^2 + (\sigma_2 - \sigma_3)^2 + (\sigma_3 - \sigma_1)^2 \right] \quad (4)$$

$$\tau_{13} = \frac{(\sigma_1 - \sigma_3)}{2} \quad (5)$$

Table 1 R -squared values for regression analysis of Drucker–Prager strength criterion and double-shear-stress strength criterion

Different stress paths	Drucker–Prager strength criterion	Double-shear-stress strength criterion
Loading stress path	0.963	0.998
Unloading stress path	0.698	0.995

$$\tau_{23} = \frac{(\sigma_2 - \sigma_3)}{2} \quad (6)$$

$$\sigma_m = \frac{1}{3} (\sigma_1 + \sigma_2 + \sigma_3) \quad (7)$$

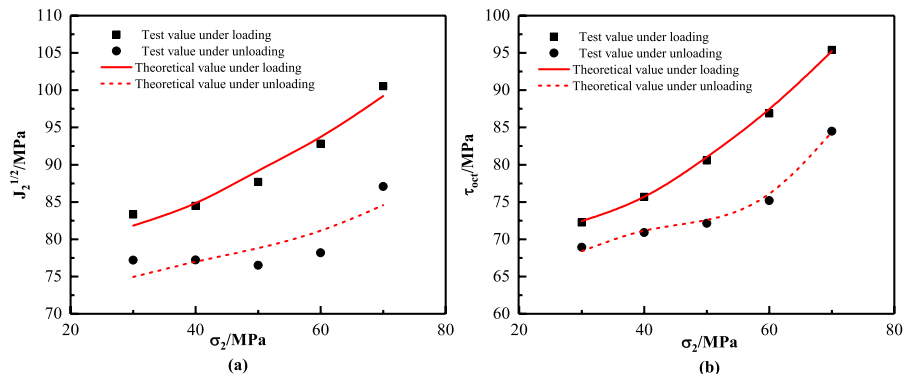
The sandstone strength regression analysis was performed by calculating each parameter in Eq. (3)–(7), and the fitted R -squared values are listed in Table 1.

By comparing the R -squared values of the two strength criteria, it is clear that the Drucker–Prager strength criterion has a better fit under the loading path than under the unloading conditions. The three-parameter double-shear-stress strength criterion delivers accurate prediction and good applicability for the strength of sandstone under loading and unloading conditions, which can reflect the yielding characteristics of sandstone strength. The specific fitting results are presented in Fig. 6.

3.3 Analysis of dilation characteristics of sandstone

The sandstone ε_v – ε_1 relationship curves (Liu et al. 2021; Zhang et al. 2019a, b) for the true-triaxial loading and unloading tests are shown in Fig. 7. It can be seen that the increase rate of ε_v accelerates with the initial σ_2 increase at the beginning of the test, but this increase then tends to decrease, and the overall volumetric strain increases first and then decreases. The maximum value of the volumetric strain is called the maximum compression volume. Volume dilatancy occurred after the volume maximum amount of compression was reached, and its degree tended to decrease, indicating that the dilation of the sandstone was suppressed, reflecting the restraining effect of the intermediate principal stress.

Fig. 6 Fitting curves of sandstone strength under **a** Drucker–Prager strength criterion and **b** double-shear-stress strength criterion



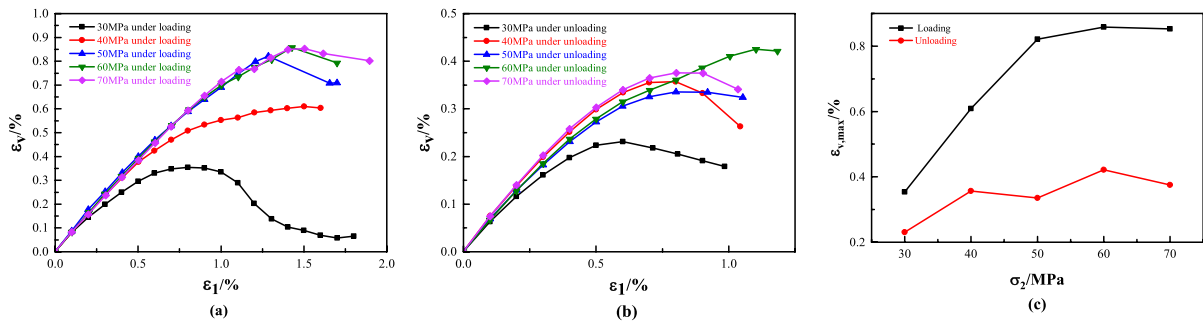


Fig. 7 Volume strain variation curves for **a** loading path and **b** unloading path. **c** Maximum volume compression point diagram for different intermediate principal stresses under loading and unloading tests

In Fig. 7, the maximum compression volumes under different intermediate principal stresses are plotted for the loading and unloading tests, respectively. The volume maximum compression for the loading test first increased rapidly with σ_2 and then stabilized, while the unloading test showed a slow increasing trend. These observations imply two findings: first, σ_2 tends to stabilize its ability to restrain the deformation of sandstone after reaching a certain value, and similar results were obtained by Brace et al. (1966) in conventional triaxial tests; second, under unloading conditions, the effect of intermediate principal stress is affected by unloading, and the effect of restraining the deformation of sandstone is substantially reduced. At the same σ_2 , the maximum volume of compression for the loading test is larger than that for the unloading test, which indicates that it is difficult for the sandstone to maintain a higher compression deformation under unloading. Although the compressive deformation becomes lower under this unloading condition, the tensile stress effect of the intermediate principal stress is released, causing dilatancy deformation in the σ_3 direction and thus dilation. This also explains the fact that sandstone undergoes stronger dilatational deformation characteristics at a lower stress state (unloading test condition) than at a higher stress state (loading test condition). Similarly, Browning et al. (2017) found that intermediate principal stresses suppress the total number of cracks and expand them to the direction of minimum principal stress, which is related to the above findings.

The onset of dilation is another aspect that needs to be considered when studying volumetric strain in sandstones. This is the point in the $(\sigma_1-\sigma_3)-\varepsilon_v$ curve at which the linear segment begins to change

into the elastic section (Haimson and Chang 2000). The $(\sigma_1-\sigma_3)-\varepsilon_v$ curve is plotted, and the onset point of dilation is labeled as D (as shown in Figs. 8 and 9), where D is the percentage of the magnitude of σ_1 corresponding to the onset point of dilation for the σ_1 peak.

In the loading test, the onset of dilation is delayed with an increase in σ_2 , but this delay gradually stabilizes. This shows that the compression deformation capacity increases with an increase in σ_2 , but its continual increase becomes difficult. In contrast, the onset point of dilation under the unloading test increased and then decreased with an increase in σ_2 , indicating that the unloading action played a role in promoting the tensile stress effect of the intermediate principal stress, which shortens the compressive deformation of sandstone after σ_2 reaches a certain value. Meanwhile, the onsets of sandstone dilation in the unloading tests all occurred earlier than those in the loading tests, which indicates that under the unloading conditions, it is difficult to maintain the compressive deformation of sandstone, and it is difficult to restrain dilation deformation owing to the reduction of the confining stress in the σ_3 direction and the tensile stress effect generated by σ_2 . This not only increases the degree of deformation in the σ_3 direction but also causes an earlier onset of dilation.

In general, the unloading test is more obvious than the loading test in terms of volume expansion, and the dilation effect is more significant. This is because the loading test σ_3 remains constant and always provides a constraint for the minimum principal stress direction. In contrast, the unloading test σ_3 -direction constraint continues to decrease and cannot balance the tensile stresses generated in the specimens. As

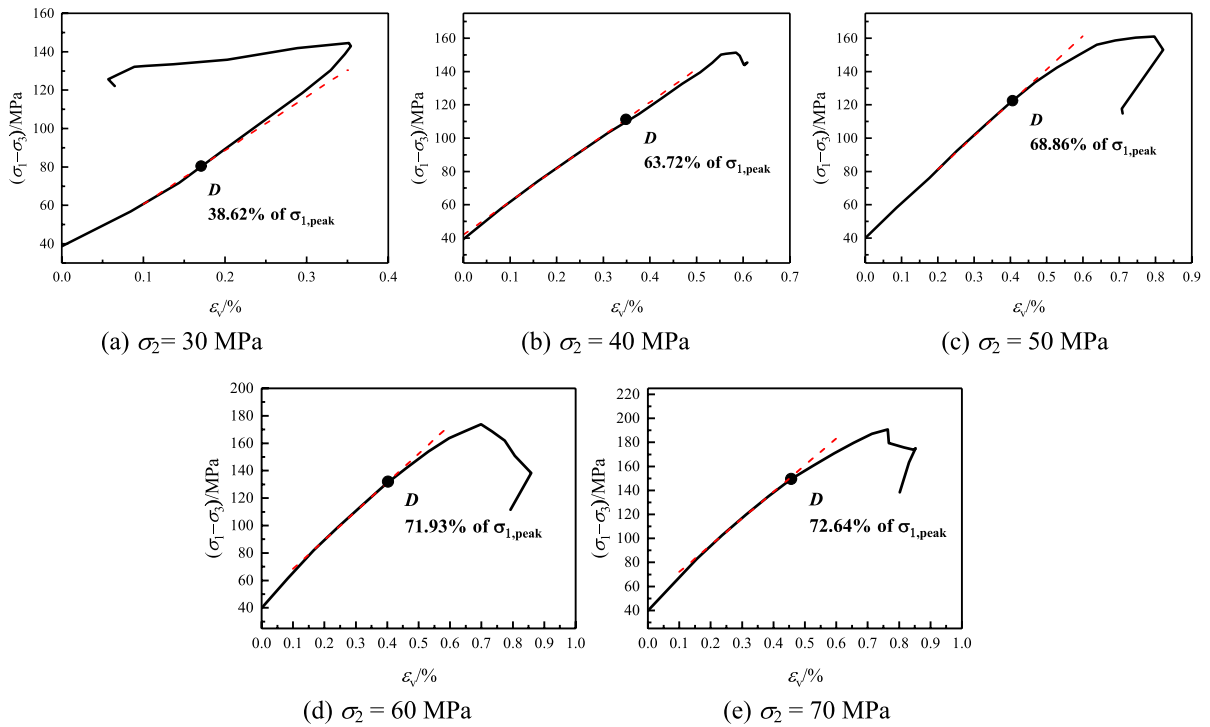


Fig. 8 Dilation onset for different intermediate principal stresses in sandstone under loading test: **a–e** $\sigma_2 = 30, 40, 50, 60,$ and 70 MPa, respectively

a result, the sandstone specimen is more likely to expand, causing an increase in the body strain and leading to an earlier and more dramatic dilation.

4 Evolution mechanisms of strain energy of sandstone under true-triaxial loading and unloading experiment

4.1 Principles of energy analysis

During the true-triaxial loading and unloading test, suppose the compressive stress is positive; in this case, the rock testing machine performs positive work on the rock in the direction of maximum principal stress and negative work in the direction of intermediate principal stress and minimum principal stress. The strain energy U of the rock contains two more parts: the releasable elastic energy U^e , which increases the elastic potential energy of the specimen, and the dissipative energy U^d , which is

generated by the internal fracture and plastic deformation of the rock. The relationship between the total energy and the elastic and dissipative energies was thus established, which are represented by the following expressions (Xie et al. 2011).

$$U = U_1 + U_2 + U_3 \quad (8)$$

$$U = U^e + U^d \quad (9)$$

In the test process, the energy absorbed in the direction of σ_1 at any moment U^1 and the negative work done in the directions of σ_2 and σ_3 U^2 and U^3 can be obtained by integrating the stress–strain curve. The relevant expressions are as follows:

$$U = U_1 + U_2 + U_3 \quad (10)$$

$$U_i = \int_0^{\varepsilon_i} \sigma_i d\varepsilon_i \quad (11)$$

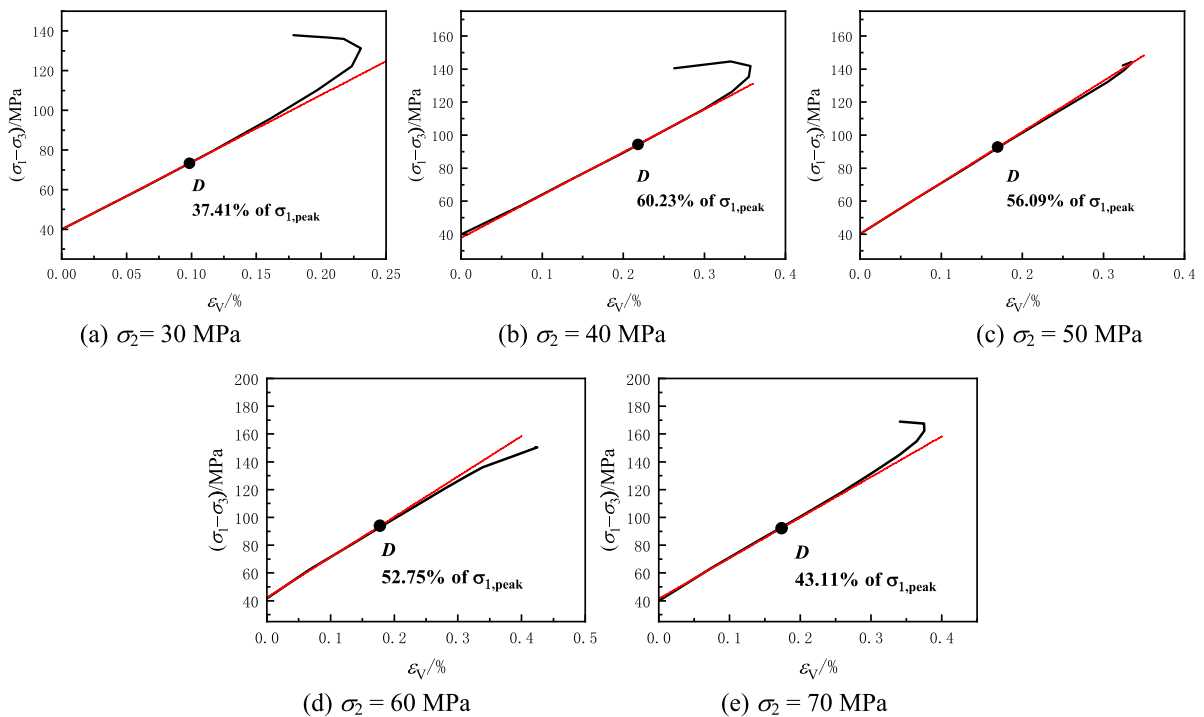


Fig. 9 Dilation onset for different intermediate principal stresses in sandstone under unloading test: **a–e** $\sigma_2=30, 40, 50, 60,$ and 70 MPa, respectively

where i is the principal stress direction. The integral of the above equation can be transformed into a differential area summation by defining the definite integral as follows:

$$U^i = \sum_{m=1}^n \frac{1}{2} (\sigma_i^m + \sigma_i^{m+1}) (\varepsilon_i^{m+1} - \varepsilon_i^m) \tag{12}$$

where m refers to the segmentation point, n to the number of micro-element areas of the stress–strain curve at time t , and the superscripts of stress σ and strain ε refer to the stress and strain at this point.

The expression for calculating the releasable elastic energy is as follows:

$$U^e = \frac{1}{2} \sigma_1 \varepsilon_1^e + \frac{1}{2} \sigma_2 \varepsilon_2^e + \frac{1}{2} \sigma_3 \varepsilon_3^e \tag{13}$$

where $\varepsilon_1^e, \varepsilon_2^e, \varepsilon_3^e$ are the elastic maximum principal strain, the elastic intermediate principal strain, and the elastic minimum principal strain, respectively. By introducing the generalized Hooke’s law, the relationship between stress and strain is obtained and introduced into Eq. (13) to obtain the computational expression for U^e as follows:

$$\varepsilon_i^e = \frac{1}{E} (\sigma_i - \nu(\sigma_j + \sigma_k)) \tag{14}$$

$$U^e = \frac{1}{2E} (\sigma_1^2 + \sigma_2^2 + \sigma_3^2 - 2\nu(\sigma_1\sigma_2 + \sigma_2\sigma_3 + \sigma_3\sigma_1)) \tag{15}$$

where E is the elastic modulus of sandstone under true-triaxial loading and unloading tests, and ν refers to the Poisson’s ratio of sandstone under true-triaxial loading and unloading tests. In this study, the energy change per unit volume of sandstone was analyzed in MJ m^{-3} .

4.2 Law of energy evolution of sandstone in different stages

The sandstone undergoes crack generation, extension, and penetration throughout the test (Li et al. 2017a, b). Accordingly, the complete stress–strain curve under true-triaxial conditions was divided into the following four stages: elastic stage (OA), microcrack stable development stage (AB), crack-accelerated expansion stage (BC), and post-peak strength-loss

stage (*CD*). In the unloading test of sandstone in this study, there is no post-peak curve, so the stress–strain curve only includes the first three stages. The energy evolution curves for the true-triaxial loading and unloading tests of sandstone under different intermediate principal stresses are obtained in Sect. 4–1. The inherent crack evolution law of sandstone deformation was analyzed according to the energy evolution law under different rock-stress stages. The details are shown in Figs. 10 and 11, respectively.

In the elastic stage, the stress–strain relationship of the specimens under loading and unloading tests was linear, most of the deformations that occurred were recoverable elastic deformations, and elastic energy dominated. In the stable development stage of micro-cracking, internal cracks of sandstone began to occur and expand under both test conditions. It is shown that the rate of increase of total energy increases, the rate of increase of elastic energy decreases, and the rate of increase of dissipation energy increases. According to the principle of maximum plastic work (Hill 1950), it is known that when the plastic deformation of the rock occurs, it is accompanied by an increase in volume. Therefore, entering into this phase often indicates the beginning of volume

expansion. In the accelerated crack expansion stage, the cracks in the loading and unloading tests expand further, plastic deformation gradually dominates, the stored releasable elastic energy begins to decline, and dissipative energy gradually takes over. In particular, the characteristic point at which the dissipative energy dominates more than the elastic energy is advanced for both tests as σ_2 increases; this tendency is the most obvious in the unloading test and will be discussed in the next section. In the post-peak damage phase, crack penetration of the specimen occurs under the loading test, the elastic energy decreases and eventually plateaus, and the dissipative energy continues to increase.

A comprehensive analysis of the energy evolution of the four stages reveals that the stage division under the loading test does not change significantly with an increase in the intermediate principal stress. However, the stage division under the unloading test shows an obvious shrinkage of the elastic stage and an increase in the plastic stage with an increase in σ_2 . Considering the stress–strain relationship of ϵ_3 in Sect. 3.1 and the law of maximum volume compression under different σ_2 in Sect. 3.3, it can be concluded that when the confining stress in the direction

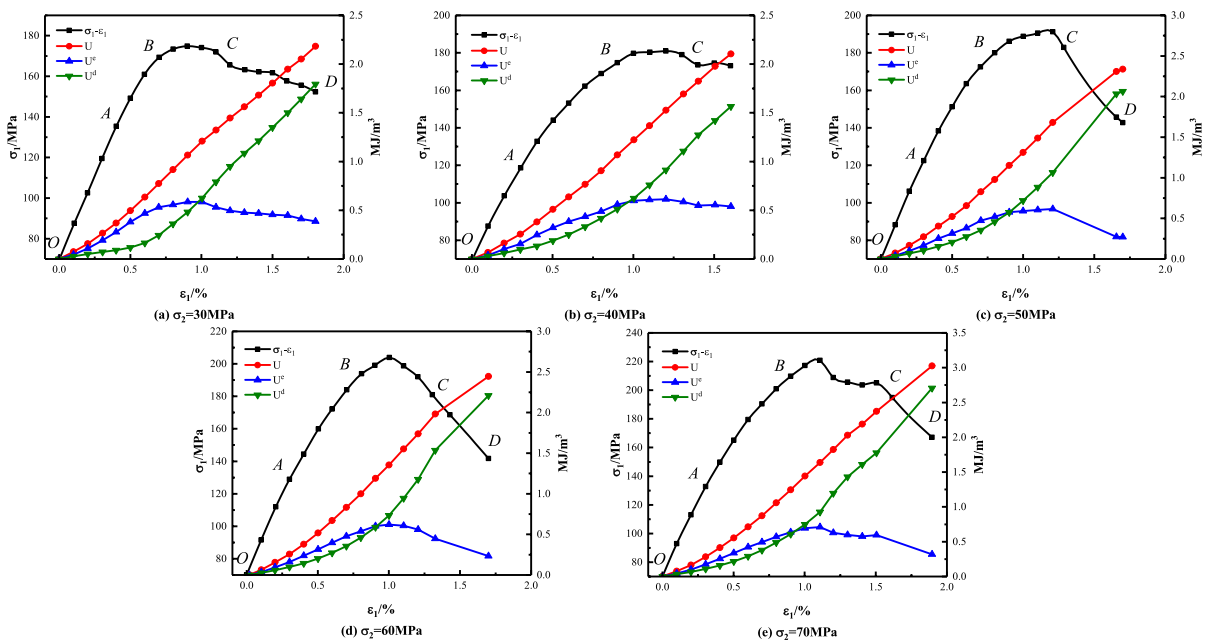


Fig. 10 Relationship between stress as well as strain energy and strain in sandstone under true-triaxial loading test conditions: **a–e** $\sigma_2 = 30, 40, 50, 60,$ and 70 MPa, respectively

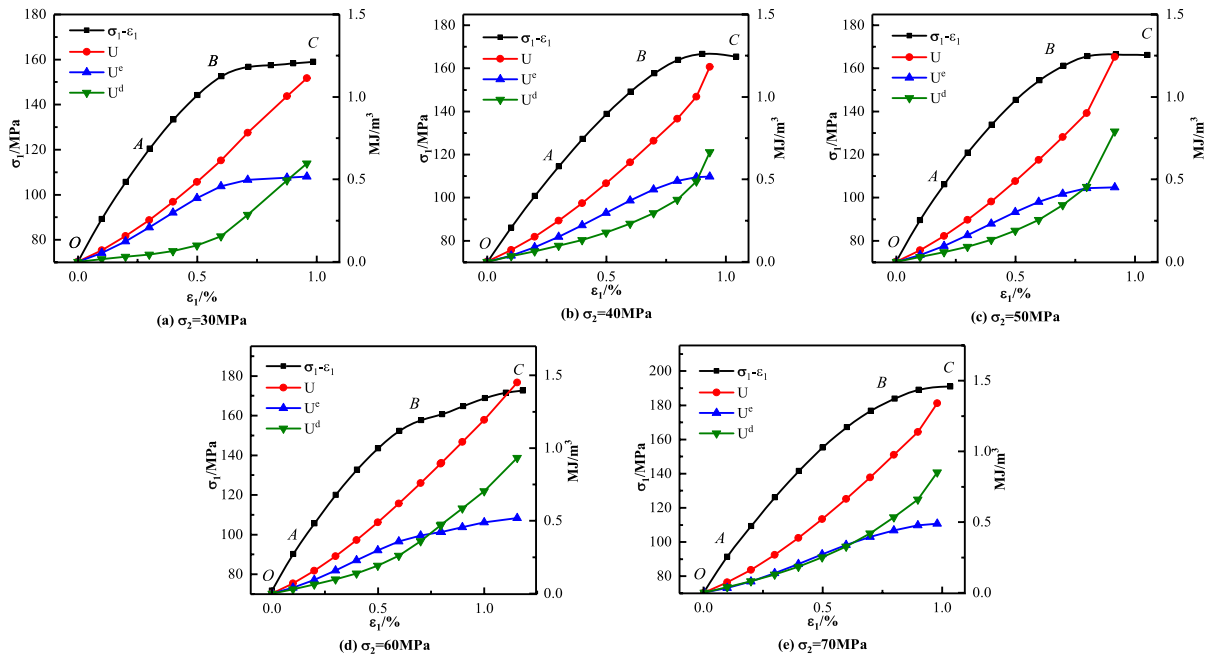


Fig. 11 Relationship between stress as well as strain energy and strain in sandstone under true-triaxial unloading test conditions: **a–e** $\sigma_2 = 30, 40, 50, 60,$ and 70 MPa, respectively

of σ_3 is maintained ($\sigma_3 = 30$ MPa), although σ_2 continues to increase, the tensile stress in the direction of σ_3 cannot overcome the constraint in the direction of σ_3 . Therefore, abundant crack formation cannot occur and significant expansion deformation results. This is consistent with the conclusions reached in Sect. 3.3. Second, the compressive deformation capacity of the sandstone is weakened when the constraint stress in the σ_3 direction decreases. Before the internal compression of the sandstone reached its limit, the expansion deformation initiated in the σ_3 direction, causing shrinkage of the elastic phase and an increase in the plastic phase. In conclusion, the intermediate principal stress effect strengthens the compressive deformation capacity of sandstone, while unloading weakens it.

4.3 Law of energy evolution for sandstone under different intermediate principal stresses

The stage analysis of energy in the previous section allows us to understand the effect of the intermediate principal stress and unloading effect of sandstone under different stress paths. However, the effects of the intermediate principal stress and unloading effects

must be analyzed more precisely. The energy evolution curves of the sandstone loading and unloading tests under different intermediate principal stress conditions are plotted in Figs. 12 and 13, respectively, and are analyzed as follows.

As σ_1 increases to the peak point, the total energy required for sandstone under the loading test was 35.40% more and 20.52% higher under the unloading test when σ_2 increased from 30 to 70 MPa. This indicates that the restraining effect and compressive deformation capacity increase as the σ_2 magnitude increases, while the unloading action weakens the compressive deformation capacity of sandstone at the same σ_2 magnitude.

In the unloading test, the accumulation rate of releasable elastic energy at the beginning of the test does not vary with the σ_2 magnitude, but its energy storage limit increases with an increase in σ_2 (Zhang et al. 2019a, b). In contrast, the rate of increase of the releasable elastic energy at the beginning of the unloading test decreases significantly with the increase in σ_2 magnitude, and its energy storage limit tends to decrease with an increase in σ_2 . This indicates that in loading tests, the restraining effect of the intermediate principal stress enhances the

Fig. 12 Energy law of true-triaxial loading test for sandstone under different intermediate principal stress conditions

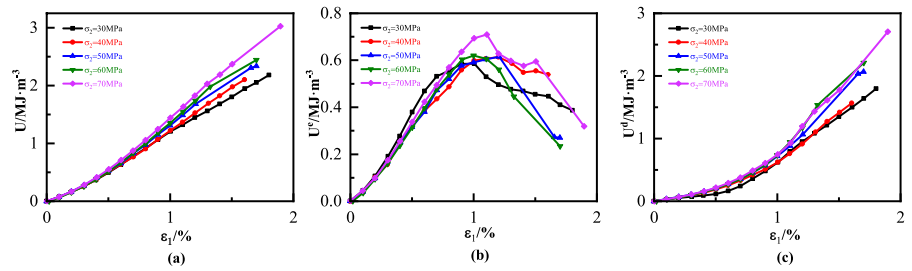
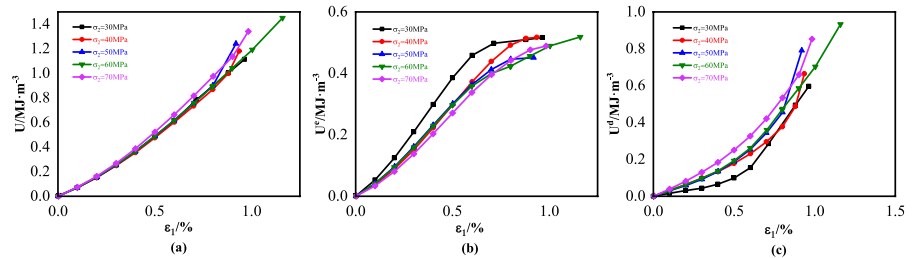


Fig. 13 Energy law of true-triaxial unloading test for sandstone under different intermediate principal stress conditions



compressive deformation capacity, but the increase is low and causes a small rate change; in the unloading tests, the unloading effect weakens the restraining effect of the intermediate principal stress, that is, with the increase in σ_2 , plastic deformation occurs before the elastic strain of the sandstone is fully developed, which reduces the elastic energy storage limit and the rate of increase. This verifies the conclusions presented in Sect. 3.3.

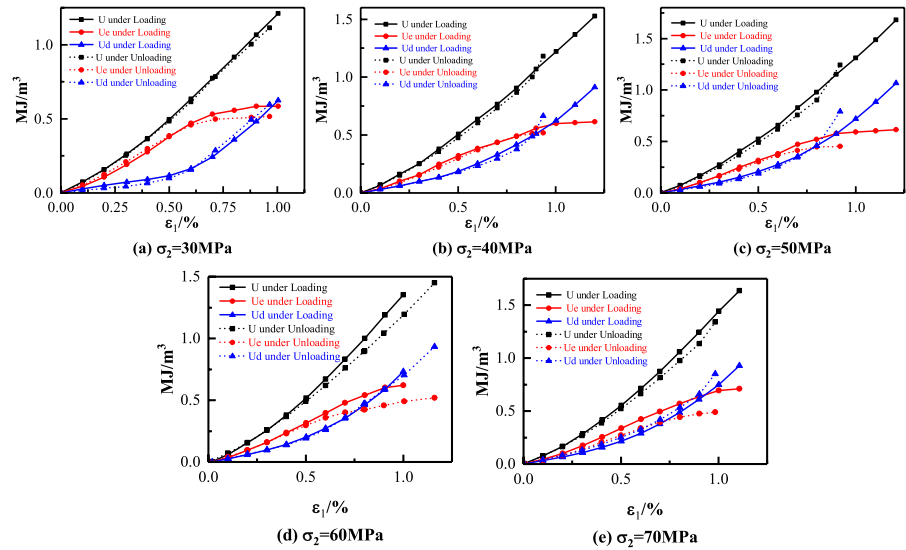
The trend of dissipative energy evolution under loading and unloading tests was basically identical, but the degree of change differed significantly. Both the initial dissipation energy share and the increase rate of the unloading test increased significantly with an increase in σ_2 magnitude, while the loading test increased slowly. It can be observed that the development of plastic deformation of sandstone under different stress paths is accelerated with an increase in σ_2 . However, the unloading action further promotes plastic deformation and crack development in the σ_3 direction, which causes the specimens to enter the crack extension stage earlier.

The energy changes in the loading and unloading tests were further compared to analyze the effect of unloading action on the deformation characteristics. The details are shown in Fig. 14.

With the evolution of energy, the total energy of the loading test before the peak was larger than that of the unloading test. This indicates that the unloading

action weakens the degree of elastic deformation, resulting in a greater decrease in elastic strain energy than the increase in dissipation energy; therefore, the total energy is lower than that of the loading test before the peak. In the figure, the unloading test exceeds the total energy of the loading test when σ_2 is 40 and 50 MPa, probably because the crack expands rapidly and the dissipation energy increases steeply, causing a sharp increase in the total energy. Comparing the releasable elastic energy of the loading and unloading tests, it was found that the initial period was basically identical, and then the elastic energy of the former became larger than that of the latter, especially after the elastic energy tended to level off. This is because the initial unloading has little effect on the specimen, microcracks have not yet been generated, and the difference in elastic energy is not large. Subsequent unloading causes the specimen to deform plastically earlier in the σ_3 direction, forming crack extension, and the specimen can accumulate less elastic energy, reflecting the unloading effect in Sect. 3.3. Comparing the dissipated energy of the loading test with that of the unloading test, it was found that the dissipated energy increased more in the latter than in the former as the test proceeded, and the characteristic point at which the percentage of dissipated energy was larger than the elastic energy occurred earlier. At $\sigma_2 = 30$ MPa and 70 MPa, the advance was 8.67% and 30.02%, respectively. With the increase in σ_2 , the

Fig. 14 Comparison of energy laws of true-triaxial loading and unloading tests on sandstone under different intermediate principal stress conditions: **a–e** $\sigma_2 = 30, 40, 50, 60,$ and 70 MPa, respectively



dissipation energy of the specimen under the unloading test increased significantly, and the plastic deformation became more obvious.

Based on the above analysis, it can be found that the change laws of the elastic and plastic phases under loading and unloading tests in the previous section correspond to those governing the energy storage limit and dissipation energy. This indicates that the unloading effect causes the elastic strain degree to decrease, and the plastic strain occurs earlier and increases, that is, the restraining effect on the intermediate principal stress is weakened and the tensile stress effect is enhanced. Combined with the findings shown in Fig. 14, it is clear that σ_3 directional unloading action promotes the generation, expansion, and penetration of microcracks, which promotes earlier plastic deformation and intensifies rock dilation. The early occurrence of the node where the dissipative energy exceeds the releasable elastic energy reflects the decrease in the restraining effect in the direction of the minimum principal stress, and the expansion of cracks in this direction and the dilation of sandstone specimens in this direction are significant compared to the loading test.

4.4 Law of energy evolution of sandstone in different directions

The σ_2 and σ_3 directions are the main directions in which expansion of the rock occurs. A further comparative analysis of the energy change of the rock

in the two directions can more intuitively reveal the effect of unloading action on the deformation of sandstone. In Sect. 4–1, the energy changes in the σ_2 and σ_3 directions were obtained and expressed by U_2 and U_3 , respectively. The specific U_2 and U_3 comparison schematics are shown in Fig. 15. In the loading test, the magnitude of U_2 was larger than that of U_3 , except for the magnitude of σ_2 , which was 30 MPa, while the opposite was true in the unloading test. The exceptions may be due to the anisotropy of the sandstone. This variation, combined with those in Fig. 3 and Eq. (11), is as follows: In both the loading and unloading tests, σ_2 is greater than σ_3 and ϵ_2 is less than ϵ_3 (under the same stress conditions). In the loading experiment, the absolute value of U_2 is greater than the absolute value of U_3 , indicating that σ_2 is greater than σ_3 determining this result; in the unloading experiment, the absolute value of U_2 is less than the absolute value of U_3 , indicating that ϵ_2 is less than ϵ_3 determining this result. This is a deeper reflection of the fact that the tensile stress effect of the intermediate principal stress under loading conditions is constrained in the σ_3 direction and cannot transcend the effect of stress on energy. On the other hand, the unloading test promotes the tensile stress effect generated by the intermediate principal stress, which causes a significant increase in its dilatational deformation beyond the effect of stress on energy, resulting in a strong dilation. This suggests that when sandstone undergoes unloading,

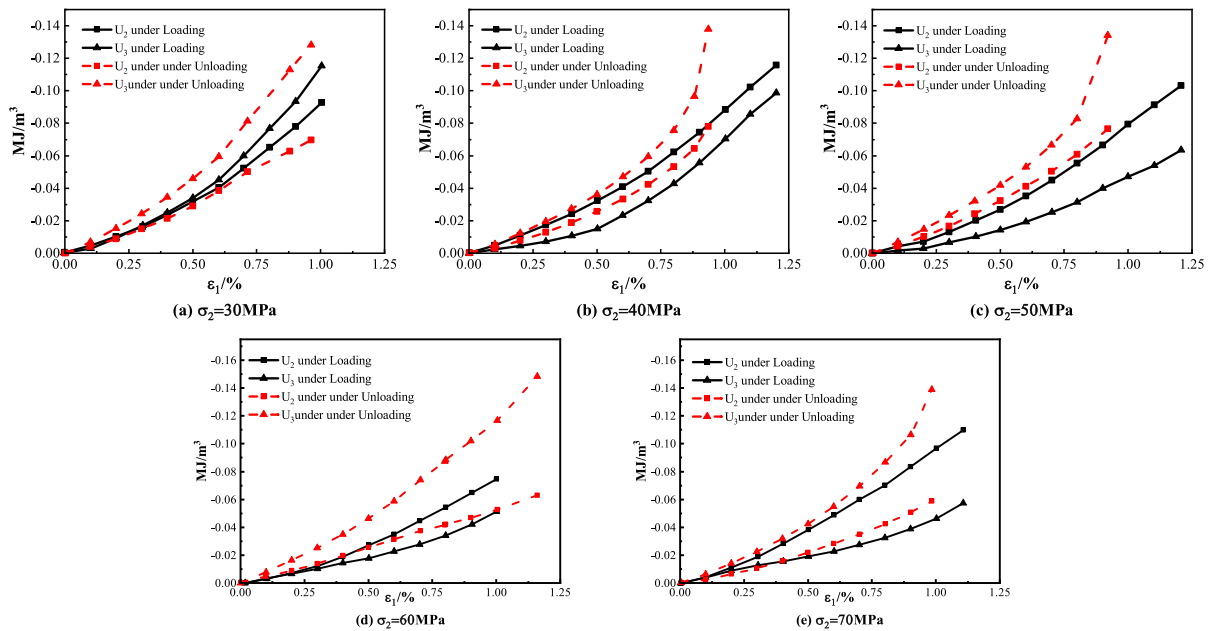


Fig. 15 Comparison of energy evolution of sandstone in the intermediate and minimum principal stress direction under true-triaxial loading and unloading test conditions: **a–e** $\sigma_2 = 30, 40, 50, 60,$ and 70 MPa, respectively

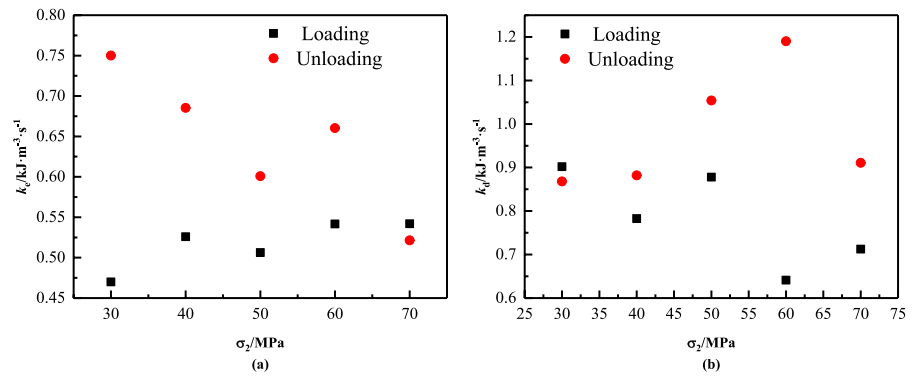
the intermediate principal stresses promote expansion and deformation on the unloading side.

Comparing the change in the size of U_2 in Fig. 15, it can be seen that the size of U_2 in the loading test is larger than that in the unloading test. This is because the unloading action weakens the intermediate principal stress constraint effect of the sandstone, and the degree of deformation in the σ_2 direction decreases. In the σ_3 direction, the unloading action strengthens the tensile stress effect of the intermediate principal stress, and the degree of deformation in the σ_3 direction increases significantly. These two aspects are consistent with the results shown in Fig. 7 and agree with the two effects of σ_2 discussed in Sect. 3.2 and with the conclusions given in Sect. 3.3. This also explains the pattern of U_3 under different tests, that is, the size of U_3 for the unloading test is larger than that for the loading test under the same ϵ_1 . This indicates that the unloading in the σ_3 direction promotes an increase in the dilatational deformation and dissipative energy in the σ_3 direction of the sandstone, which results in a significant dilation of the sandstone.

4.5 Characteristics of the average energy conversion rate of sandstone

Dilation is not only accompanied by plastic deformation but also the release of elastic energy (Li 2001; Tarasov and Stacey 2017). Comparing the magnitude of strain energy under loading and unloading conditions and analyzing the energy evolution in different directions can reveal the deformation characteristics of sandstone, but it is not possible to visually analyze the energy conversion efficiency, much less to determine the course of sandstone deformation. By considering the time effect of the energy evolution of the specimen, it is possible to reflect the characteristics of the specimen deformation and crack extension. Therefore, the amount of releasable elastic energy and dissipative energy change with time is important for revealing the dilation properties of rocks. In this study, the average strain energy conversion rate is defined as the ratio of the strain energy increment to the time increment. The average elastic strain energy conversion rate (k_e) and the average dissipative energy conversion rate (k_d) are given by Eq. (16) and (17). ΔU^e is the elastic strain energy corresponding

Fig. 16 Changes of average elastic and dissipative energy conversion rate in sandstone under true-triaxial loading and unloading test conditions: **a** average elastic energy conversion rate and **b** average dissipative energy conversion rate



to the peak point minus the elastic strain energy corresponding to the initial point of strain measurement, ΔU^d is the dissipation energy corresponding to the peak point minus the dissipation energy corresponding to the initial point of strain measurement, and Δt is the loading time corresponding to the peak point minus the loading time corresponding to the initial point of strain measurement. The average elastic energy conversion rate and the average dissipation energy conversion rate under loading and unloading conditions are shown in Fig. 16.

$$k_e = \frac{\Delta U^e}{\Delta t} \tag{16}$$

$$k_d = \frac{\Delta U^d}{\Delta t} \tag{17}$$

Excluding the fluctuation of some points, it was found that k_e essentially becomes an increasing trend and k_d essentially decreases with an increase in σ_2 under the loading test, but both trends are very slow to develop. However, under the unloading test, the opposite trend is observed, and the change is more obvious than in the loading condition. Furthermore, combined with the conclusion obtained in Sect. 4.3, the energy storage limit and the magnitude of dissipated energy at the peak increase with σ_2 under the loading test. The comprehensive analysis shows that with the increase in intermediate principal stress, the accumulation of releasable elastic energy is more rapid, while the dissipation energy evolves less drastically and the course increases substantially, reflecting a certain tendency of ductile deformation in sandstone. However, unloading conditions break this mechanical deformation property (as outlined in Sect. 4.3); not only does

the average elastic strain energy conversion rate and the energy storage limit decrease, but they also cause the average dissipative energy conversion rate and its total amount to increase. Therefore, there is a more drastic change in the dissipation energy in the unloading test, reflecting the brittle deformation tendency of sandstone. The reason for the two different deformation tendencies produced by the loading and unloading tests is that σ_3 is a constant value under the loading test; the change in its tensile stress effect is not obvious, and the degree of deformation for increasing plastic expansion in the σ_3 direction is low. While the unloading test under the strengthening of the intermediate principal stress in the σ_3 direction produced the effect of tensile stress, sandstone fracture expansion accelerated, showing a brittle damage tendency.

In addition, the average elastic energy conversion rate and the average dissipative energy conversion rate under the unloading test were larger than those under the loading condition. Combined with Fig. 14, because the elastic energy of the unloading test is smaller than that of the loading test, whereas k_e is larger than that of the loading test, the total amount of elastic energy in the unloading test is small and the accumulation rate is large, so the accumulation of the main elastic energy can be completed quickly and the course will be very short. This reflects the weakening of the elastic compression deformation caused by the unloading action. Meanwhile, Sect. 4.3 demonstrated that the dissipation energy of the unloading test exceeds that of the loading test near the peak point. Combined with the result that the k_d of the unloading test was greater than that under the loading test, it was concluded that the dissipation energy of the sandstone specimens under unloading conditions

increased rapidly, the crack expansion was more violent, and the resulting dilation was more pronounced. These observations indicate that unloading enhances the effect of the tensile stresses generated by the intermediate principal stresses.

In summary, the unloading effect not only accelerates the development of plastic dilatancy deformation and advances its occurrence but also accelerates the completion of elastic compression deformation. Therefore, the weakening of the unloading effect for the intermediate principal stress constraint effect is manifested in the shortening of the compressive deformation course, while the strengthening of the intermediate principal stress tensile stress effect is manifested in the promotion of the degree of plastic expansion deformation development.

5 Conclusions

Under true-triaxial excavation conditions, the surrounding sandstone body undergoes dilation. To clearly analyze the dilation characteristics, the intermediate principal stress restraining effect and tensile stress effect, as well as the effect of unloading action on these two effects, were investigated. It was found that when the minimum principal stress is constant ($\sigma_3 = 30$ MPa), the intermediate principal stress restraining effect strengthened and stabilized as σ_2 increased, while the tensile stress had little effect. Under the unloading effect, the intermediate principal stress constraint effect decreases, while the tensile stress effect strengthens. These findings are useful for guiding the orderly conduct and development of actual excavation works. Within the scope of this study, the following conclusions can be drawn based on the experimental results.

(1) With an increase in the intermediate principal stress, the volume maximum compression increases, the onset of dilation is delayed in the loading test, and both eventually level off; in the unloading test, the volume maximum compression increases slowly, and the onset of dilation is first delayed and then occurs in advance. The unloading test is more obvious than the loading test in terms of volume expansion, and the dilation effect is more significant.

- (2) Under the loading test, the energy storage limit increases with an increase in the intermediate principal stress, whereas under the unloading test, the law is the opposite. The trend of dissipative energy evolution under the two test conditions was basically identical, but the characteristic point at which the dissipative energy accounted for more than the elastic energy in the unloading test appeared earlier than that in the loading test.
- (3) The energy magnitude in the σ_2 direction is larger than that in the σ_3 direction in the loaded test, whereas the opposite is true in the unloaded test. Under different intermediate principal stress conditions, the size of U_2 in the loaded test was larger than that in the unloaded test, whereas the size of U_3 in the loaded test was smaller than that in the unloaded test.
- (4) A comprehensive analysis of the average elastic energy conversion rate and the average dissipative energy conversion rate under different test conditions revealed that the weakening of the unloading effect on the restraining effect of the intermediate principal stress is manifested by shortening the compressive deformation course. The strengthening of the tensile stress effect on the intermediate principal stress is manifested by promoting the degree of plastic expansion deformation development.

Acknowledgements This work was supported by Distinguished Youth Funds of National Natural Science Foundation of China (No. 51925402), National Science Foundation for Young Scientists of China (No. 51804211, 52004170, No52104176), Fundamental Research Program of Shanxi (No. 201901D211037), State Key Laboratory Cultivation Base for Gas Geology and Gas Control (Henan Polytechnic University) (No. WS2019B04), Scientific and Technological Innovation Programs of Higher Education Institutions in Shanxi (No. 2020L0067).

Author contributions WL and ZW wrote the main manuscript text; GF was mainly involved in the content improvement and revision of the article; HZ, JD, HL and MD prepared Figs. 1, 2, 3, 4, 5, 6, 7, 8, 9, 10, 11, 12, 13, 14, 15, 16 and Table 1. All authors reviewed the manuscript.

Funding This work was supported by Distinguished Youth Funds of National Natural Science Foundation of China (No. 51925402), National Science Foundation for Young Scientists of China (No. 51804211, 52004170, No52104176), Fundamental Research Program of Shanxi (No. 201901D211037), State

Key Laboratory Cultivation Base for Gas Geology and Gas Control (Henan Polytechnic University) (No. WS2019B04), Scientific and Technological Innovation Programs of Higher Education Institutions in Shanxi (No. 2020L0067).

Data availability The data that support the findings of this study are available from the corresponding author (Guorui Feng) upon reasonable request.

Declarations

Ethics approval and consent to participate There are no ethical issues related to the research in this paper.

Consent to publish Not applicable.

Competing interests On behalf of all authors, the corresponding author states that there is no conflict of interest.

Open Access This article is licensed under a Creative Commons Attribution 4.0 International License, which permits use, sharing, adaptation, distribution and reproduction in any medium or format, as long as you give appropriate credit to the original author(s) and the source, provide a link to the Creative Commons licence, and indicate if changes were made. The images or other third party material in this article are included in the article's Creative Commons licence, unless indicated otherwise in a credit line to the material. If material is not included in the article's Creative Commons licence and your intended use is not permitted by statutory regulation or exceeds the permitted use, you will need to obtain permission directly from the copyright holder. To view a copy of this licence, visit <http://creativecommons.org/licenses/by/4.0/>.

References

- Ai C, Zhang J, Li Y, Zeng J, Yang X, Wang J (2016) Estimation criteria for rock brittleness based on energy analysis during the rupturing process. *Rock Mech Rock Eng* 49:4681–4698. <https://doi.org/10.1007/s00603-016-1078-x>
- Alejano LR, Alonso EE (2005) Considerations of the dilatancy angle in rocks and rock masses. *Int J Rock Mech Min Sci* 42:481–507. <https://doi.org/10.1016/j.ijrmms.2005.01.003>
- Alexeev AD, Revva VN, Bachurin LL, Prokhorov IY (2008) The effect of stress state factor on fracture of sandstones under true-triaxial loading. *Int J Fract* 149:1–10. <https://doi.org/10.1007/s10704-008-9214-6>
- Brace WF, Paulding BW, Scholz CH (1966) Dilatancy in the fracture of crystalline rocks. *J Geophys Res* 71:3939–3953. <https://doi.org/10.1029/JZ071i016p03939>
- Browning J, Meredith PG, Stuart CE, Healy D, Harland S, Mitchell TM (2017) Acoustic characterization of crack damage evolution in sandstone deformed under conventional and true-triaxial loading. *J Geophys Res Solid Earth* 122:4395–4412. <https://doi.org/10.1002/2016JB013646>
- Chen Z, Su G, Ju JW, Jiang J (2019) Experimental study on energy dissipation of fragments during rockburst. *Bull Eng Geol Environ* 78:5369–5386. <https://doi.org/10.1007/s10064-019-01463-9>
- Drucker DC, Prager W (1952) Soil mechanics and plastic analysis or limit design. *Quart Appl Math* 10:157–165. <https://doi.org/10.1090/qam/48291>
- Duan M, Jiang C, Gan Q, Li M, Peng K, Zhang W (2020) Experimental investigation on the permeability, acoustic emission and energy dissipation of coal under tiered cyclic unloading. *J Nat Gas Sci Eng* 73:103054. <https://doi.org/10.1016/j.jngse.2019.103054>
- Feng F, Chen S, Wang Y, Huang W, Han Z (2021a) Cracking mechanism and strength criteria evaluation of granite affected by intermediate principal stresses subjected to unloading stress state. *Int J Rock Mech Min Sci*. <https://doi.org/10.1016/j.ijrmms.2021.104783>
- Feng X, Zhang J, Yang C, Tian J, Lin F, Li S, Su X (2021b) A novel true-triaxial test system for microwave-induced fracturing of hard rocks. *J Rock Mech Geotech Eng* 13:961–971. <https://doi.org/10.1016/j.jrmge.2021.03.008>
- Gao Y, Tao Z (1993) True-triaxial pressure test inspection and analysis of rock strength criterion (in Chinese). *J Geotech Eng* 04:26–32
- Haimson BC, Chang C (2000) A new true-triaxial cell for testing mechanical properties of rock, and its use to determine rock strength and deformability of Westerly granite. *Int J Rock Mech Min Sci* 37:285–296. [https://doi.org/10.1016/S1365-1609\(99\)00106-9](https://doi.org/10.1016/S1365-1609(99)00106-9)
- Handin JW, Heard HC, Magouirk JN (1967) Effect of the intermediate principal stress on the failure of limestone, dolomite, and glass at different temperature and strain rate. *J Geophys Res* 72:611–640. <https://doi.org/10.1029/JZ072i002p00611>
- Hill R (1950) *The mathematical theory of plasticity*. Oxford University Press, Oxford
- Jiang Q, Zhang M, Yan F, Su G, Feng X, Xu D, Feng G (2021) Effect of initial minimum principal stress and unloading rate on the spalling and rockburst of marble: a true-triaxial experiment investigation. *Bull Eng Geol Environ* 80:1617–1634. <https://doi.org/10.1007/s10064-020-01995-5>
- Kaiser PK, Diederichs MS, Martin CD, Sharp J, Steiner W (2000) Underground works in hard rock tunnelling and mining. In: *Proceedings of the GeoEng 2000 Conference*, Technomic Publishers Co Inc, Lancaster, pp 841–926
- Kie T, Quan S, Hai Y, Yang W (1989) Dilatancy, creep and relaxation of brittle rocks measured with the 8000 kN multipurpose triaxial apparatus. *Phys Earth Planet Inter* 55:335–352. [https://doi.org/10.1016/0031-9201\(89\)90081-2](https://doi.org/10.1016/0031-9201(89)90081-2)
- Lau JSO, Chandler NA (2004) Innovative laboratory testing. *Int J Rock Mech Min Sci* 41:1427–1445. <https://doi.org/10.1016/j.ijrmms.2004.09.008>
- Li Q (2001) Strain energy density failure criterion. *Int J Solids Struct* 38:6997–7013. [https://doi.org/10.1016/S0020-7683\(01\)00005-1](https://doi.org/10.1016/S0020-7683(01)00005-1)
- Li M, Yin G, Xu J, Li W, Song Z, Jiang C (2016) A novel true-triaxial apparatus to study the geomechanical and fluid

- flow aspects of energy exploitations in geological formations. *Rock Mech Rock Eng* 49:4647–4659. <https://doi.org/10.1007/s00603-016-1060-7>
- Li D, Sun Z, Xie T, Li X, Ranjith PG (2017a) Energy evolution characteristics of hard rock during triaxial failure with different loading and unloading paths. *Eng Geol* 228:270–281. <https://doi.org/10.1016/j.enggeo.2017.08.006>
- Li J, Wang M, Xia K, Zhang N, Huang H (2017b) Time-dependent dilatancy for brittle rocks. *J Rock Mech Geotech Eng* 9:1054–1070. <https://doi.org/10.1016/j.jrmge.2017.08.002>
- Liu J, Zhang L, Cong Y, Wang Z (2021) Research on the mechanical characteristics of granite failure process under true-triaxial stress path. *Rock Soil Mech* 08:2069–2077. <https://doi.org/10.16285/j.rsm.2021.0110>
- Liu S, Zheng H, Chen G, Hu Y, Meng K (2023) Acoustic emission precursor information of rock failure under true triaxial loading and unloading conditions. *Front*. <https://doi.org/10.3389/feart.2023.1182413>
- Lu J, Yin G, Zhang D, Gao H, Li C, Li M (2020a) True-triaxial strength and failure characteristics of cubic coal and sandstone under different loading paths. *Int J Rock Mech Min Sci* 135:104439. <https://doi.org/10.1016/j.ijrmms.2020.104439>
- Lu J, Zhang D, Huang G, Li X, Gao H, Yin G (2020b) Effects of loading rate on the compound dynamic disaster in deep underground coal mine under true-triaxial stress. *Int J Rock Mech Min Sci* 134:104453. <https://doi.org/10.1016/j.ijrmms.2020.104453>
- Ma X, Haimson BC (2016) Failure characteristics of two porous sandstones subjected to true-triaxial stresses. *J Geophys Res Solid Earth* 121:6477–6498. <https://doi.org/10.1002/2016JB012979>
- Mogi K (1967) Effect of the intermediate principal stress on rock failure. *J Geophys Res* 72:5117–5131. <https://doi.org/10.1029/JZ072i020p05117>
- Mogi K (1971) Fracture and flow of rocks under high triaxial compression. *J Geophys Res* 76:1255–1269. <https://doi.org/10.1029/JB076i005p01255>
- Si X, Gong F (2020) Strength-weakening effect and shear-tension failure mode transformation mechanism of rockburst for fine-grained granite under triaxial unloading compression. *Int J Rock Mech Min Sci*. <https://doi.org/10.1016/j.ijrmms.2020.104347>, 104347
- Song Z, Li M, Yin G, Ranjith PG, Zhang D, Liu C (2018) Effect of intermediate principal stress on the strength, deformation, and permeability of sandstone. *Energies*. <https://doi.org/10.3390/en11102694>
- Tarasov BG, Stacey TR (2017) Features of the energy balance and fragmentation mechanisms at spontaneous failure of class I and class II rocks. *Rock Mech Rock Eng* 50:2563–2584. <https://doi.org/10.1007/s00603-017-1251-x>
- Walton G, Arzúa J, Alejano LR, Diederichs MS (2015) A laboratory-testing-based study on the strength, deformability, and dilatancy of carbonate rocks at low confinement. *Rock Mech Rock Eng* 48:941–958. <https://doi.org/10.1007/s00603-014-0631-8>
- Wang G, Feng X, Yang C, Zhao J, Xiong Y, Wang J (2023a) Effect of lateral stress on shear strength of jointed hard rocks in true triaxial single-shear test. *Bull Eng Geol Environ* 82:1–14. <https://doi.org/10.1007/s10064-023-03479-8>
- Wang Y, Du W, Zhang D, Yu B (2023b) Effect of loading and unloading rates on sandstone deformation and dilatancy under true triaxial condition. *Sustainability*. <https://doi.org/10.3390/su15065105>
- Wen Z, Wang X, Tan Y, Zhang H, Huang W, Li Q (2016) A study of rockburst hazard evaluation method in coal mine. *Shock Vib* 2016:1–9. <https://doi.org/10.1155/2016/8740868>
- Wu W, Gong F, Yang W (2020) Experimental simulation study of spalling in deep rectangular tunnel with plastic fine grain marble. *Tunn Undergr Space Technol* 98:103319. <https://doi.org/10.1016/j.tust.2020.103319>
- Xie H, Li L, Ju Y, Peng R, Yang Y (2011) Energy analysis for damage and catastrophic failure of rocks. *Sci China Technol Sci* 54:199–209
- Xie H, Ju Y, Gao F, Gao M, Zhang R (2017) Groundbreaking theoretical and technical conceptualization of fluidized mining of deep underground solid mineral resources. *Tunn Undergr Space Technol* 67:68–70. <https://doi.org/10.1016/j.tust.2017.04.021>
- Zhai S, Su G, Yin S, Yan S, Wang Z, Yan L (2020) Fracture evolution during rockburst under true-triaxial loading using acoustic emission monitoring. *Bull Eng Geol Environ* 79:4957–4974. <https://doi.org/10.1007/s10064-020-01858-z>
- Zhang Y, Feng X, Zhang X, Wang Z, Sharifzadeh M, Yang C (2019a) A novel application of strain energy for fracturing process analysis of hard rock under true-triaxial compression. *Rock Mech Rock Eng* 52:4257–4272. <https://doi.org/10.1007/s00603-019-01868-8>
- Zhang Y, Feng X, Zhang X, Wang Z, Sharifzadeh M, Yang C, Kong R, Zhao J (2019b) Strain energy evolution characteristics and mechanisms of hard rocks under true-triaxial compression. *Eng Geol*. <https://doi.org/10.1016/j.enggeo.2019.105222>
- Zhao X, Cai M (2010) Influence of plastic shear strain and confinement-dependent rock dilation on rock failure and displacement near an excavation boundary. *Int J Rock Mech Min Sci* 47:723–738. <https://doi.org/10.1016/j.ijrmms.2010.04.003>
- Zheng Z, Feng X (2020) Influence of intermediate principal stress on the mechanical properties of rocks containing fractures. *Geotech Lett* 10:82–87. <https://doi.org/10.1680/jgele.19.00092>

Publisher's Note Springer Nature remains neutral with regard to jurisdictional claims in published maps and institutional affiliations.